Superplastic behaviour of an Al–Li–Cu–Mg alloy

R. Kaibyshev*[1] and O. Osipova[1]

The superplastic properties and microstructure evolution of an Al–Li–Cu–Mg alloy were examined in tension in the temperature interval 400–525°C at strain rates ranging from $1{\cdot}4\times10^{-4}$ to $5{\cdot}6\times10^{-2}$ s^{-1}. The refined microstructure with an average grain size of about 11 μm was produced in thin sheets by a thermomechanical processing. A maximum elongation to failure of 960% appeared at a temperature of 475°C and an initial strain rate of $1{\cdot}4\times10^{-3}$ s^{-1}, with corresponding strain sensitivity coefficient m of about 0·58. The highest m value was approx. 0·64 at the similar strain rate and T=525°C ($\delta\approx750\%$). The microstructural evolution during superplastic deformation of the Al–Li–Cu–Mg alloy has been studied quantitatively. The role of dispersoids in superplasticity is considered.

Keywords: Aluminium alloy, Fine-grained structure, Thermomechanical processing, Superplasticity, Microstructure, Dispersoids

Introduction

Al–1·9%Li–1%Mg–1·7%Cu alloy containing nanoscale $Al_3(Sc,Zr)$ dispersoids is an attractive material for aerospace applications because of its excellent combination of high strength, superior crack propagation resistance and workability at room temperature.[1,2] This alloy was designated in the Former Soviet Union as 1443 Al. The 1443 Al is a single Al–Li alloy that can be processed into thin sheets with a thickness of 0·5 mm by cold rolling. As a result, this alloy is considered as an advanced sheet material for fuselage skin of civil airplanes.[1] Currently there is a great interest in making superplastic Al–Li–Cu–Mg alloys in order to build monolithic structures for airframes through superplastic blow forming (SPF).[3–6] However, at present, only marginal superplastic properties have been attained in 1443 Al.[3,4]

It is known that Al–Li–Cu–Mg alloys can exhibit superplasticity in two distinctly different microstructural conditions. First, these alloys exhibit superplastic behaviour in the recrystallised condition.[2,5,7–9] The fine grained structure with a mean grain size less than 10 μm is produced by two-step thermomechanical processing (TMP).[5] The first step involves solution treatment followed by water quenching and subsequent overaging to develop large particles of T-phase (Al_2CuLi (T_1) or/and Al_7Cu_4Li (T_B)) or/and S-phase (Al_2CuMg).[5] Next, after warm or cold working a rapid recrystallisation treatment is used to produce a fully recrystallised structure.[5,10] Second phase dispersoids pin high-angle boundaries and so stabilise recrystallised structure under static annealing and superplastic deformation.[5,10] This TMP was termed as overaging/recrystallisation TMP.[11] Second, Al–Li–Cu–Mg alloys exhibited superplasticity in initial unrecrystallised condition.[6,12] An Al–Li–Cu–Mg alloy containing a dispersion of Al_3Zr particles was subjected to extensive warm rolling followed by heating to temperatures of superplastic deformation.[6] Initial unrecrystallised structure consisting of cells or recovered subgrains gradually transforms into fine grained structure during the initial stages of superplastic deformation by continuous recrystallisation.[5,6,10] Al_3Zr particles prevent static recrystallisation in worked material by exerting a drag on the climbing dislocation and subboundaries under static annealing.[5,6,10] However, these dispersoids cease to be effective in restraining dislocation migration under superplastic deformation at high temperature, and fine grained structure is evolved through continuous dynamic recrystallisation.[5,6,10,11,13]

It was recently shown that aluminium–lithium alloys in recrystallised conditions exhibit enhanced superplastic properties in comparison with warm worked material.[14] The presence of Sc and Zr in an Al–Li alloy stabilises fine-grained structure. In principle, the phase composition of the 1443 Al permits the use of overaging to develop large (≈1 μm) secondary precipitates from the T_B-phase prior to working. These particles can provide inhomogeneous deformation during warm rolling in addition to acting as nucleation sites for new grains during subsequent recrystallisation annealing.[5,10] However, it was found previously that the use of overaging in this material has no remarkable advantageous because overaging results in plate shaped particles from the T_B-phase, which do not provide homogeneous nucleation during subsequent recrystallisation.[15] In addition, the overaging/recrystallisation TMP is very complicated and difficult to be implemented in practice. To overcome this restriction, a TMP route was developed to produce a uniform grain structure (≈11 μm) in the 1443 Al. The aim of the present study

[1]Institute for Metals Superplasticity Problems, Khalturina 39, Ufa 450001, Russia

*Corresponding author, email rustam@anrb.ru

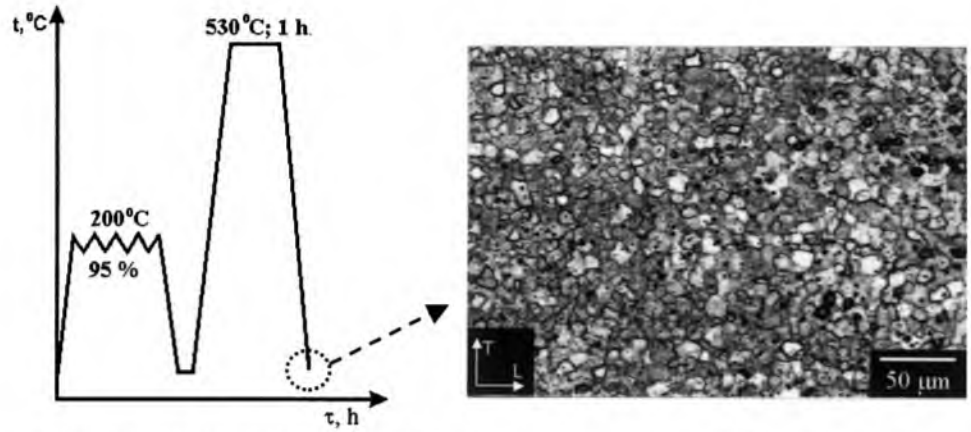

1 Schematic representation of TMP used to produce fine-grained structure in the 1443 Al and typical microstructures after TMP

is to examine superplastic behaviour of the 1443 Al with this structure.

Material and experimental procedure

The 1443 Al with chemical composition Al–1·9Li–1Mg–0·03Sc–1·7Cu–0·08Zr (wt-%) was manufactured at the Kamensk–Urals Metallurgy Plant by direct chill casting. The ingot with 360 mm diameter and 680 mm height was solution heat treated at 530°C for 20 h followed by air cooling. Plates with rectangular cross-sections and dimensions $50 \times 30 \times 20$ mm were machined from the central part of the ingot parallel to the major axis. The alloy was then subjected to recrystallisation TMP (Fig. 1). The plates were re-heated at 530°C for 1 h followed by water quenching. Next, the plates were heated at $T=200$°C and then, rolled to a final thickness of 1 mm, giving a total reduction of 95% in 20 passes. A four-high mill with isothermal internal rollers of 160 mm in diameter and 200 mm in length was used. The internal rollers were heated and kept at $T=200$°C during rolling. Final recrystallisation annealing was carried out at $T=530$°C in a salt bath for 1 h followed by water quenching.

Following the TMP, tensile samples were machined parallel to the rolling direction with gauge lengths of 6 mm and cross-sectional dimensions of 1×3 mm^2. Tensile tests were performed at strain rates ranging from $1{\cdot}4 \times 10^{-4}$ to $5{\cdot}6 \times 10^{-2}$ s^{-1} in the temperature interval 400–525°C. Other details of the mechanical test were reported earlier.[11,15]

Microstructures were revealed by etching with standard Keller solution. Cavitation was measured within the sample body to avoid the effect of surface diffusion by the metallography technique.[15] For this purpose, the surface layer of ≈0·5 mm thickness was eliminated by mechanical polishing. Areas of specimens strained up to failure (located 5 mm from the fracture surface) were examined. All samples for metallography and cavitation studies were strained at $1{\cdot}4 \times 10^{-3}$ s^{-1}. Other details of microstructure characterisation and cavitation study were reported earlier.[3,4,15]

Experimental results

Microstructure after TMP

TMP resulted in the formation of a uniform structure with an average grain size of about 11 μm (Fig. 1). Particles with an equiaxed shape and an average size of about 34 nm were found within interiors of recrystallised grains (Fig. 2). The nature of these dispersoids is probably $Al_3(Zr,Sc)$. About 92% of them exhibit incoherent boundaries (Fig. 2). Several dispersoids exhibited the specific 'bean-coffee' contrast suggesting their coherent origin. In addition, coarse particles from the S-phase with an equiaxed shape are present in the resulting structure (Fig. 1). However, their volume fraction is negligible (≈0·5%).

Superplastic behaviour

The typical true stress–true strain (σ–ε) curves for the 1443 Al at an initial strain rate of $1{\cdot}4 \times 10^{-3}$ s^{-1} and temperatures ranging from 400 to 525°C are shown in Fig. 3*a*. Figure 3*b* shows the σ–ε curves at a temperature of 475°C and strain rates ranging from $1{\cdot}4 \times 10^{-4}$ to $5{\cdot}6 \times 10^{-2}$ s^{-1}. Two types of σ–ε curves can be distinguished. At low temperature and high strain rates, extensive strain hardening takes place initially. After reaching a maximum stress, the flow stress continuously decreases until failure. A well-defined peak in flow stress is observed and no steady state flow occurs. At higher temperatures and lower strain rates, the complex shape of the σ–ε curves is observed. A gradual strain hardening takes place up to high strains. An increase in temperature or a decrease in strain rate results in an increase in initial work hardening. Apparent steady state flow can be distinguished at $\varepsilon \geqslant 1{\cdot}2$. Secondary strain hardening was found at the similar conditions after the apparent steady state flow. At all of the temperatures

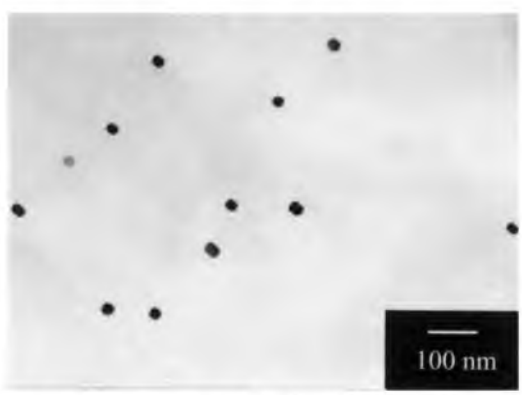

2 Initial microstructure of the 1443 Al after TMP

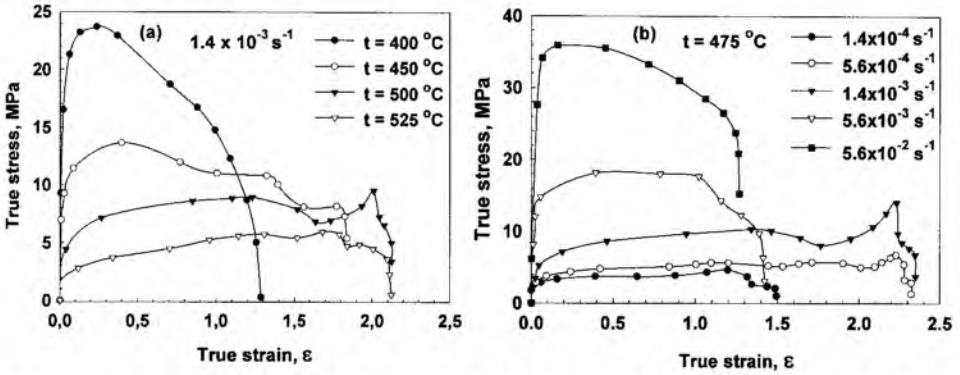

3 (a) Effect of temperature on true stress–strain curves at an initial strain rate of $1{\cdot}4\times10^{-3}\ s^{-1}$; (b) effect of strain rate on true stress–strain curves at 475°C

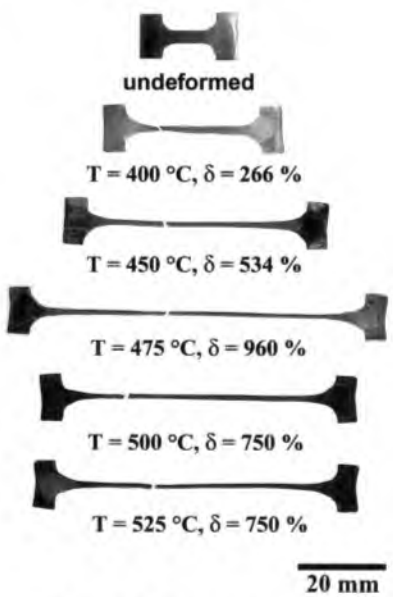

4 Shadowgraphs of the fracture in samples pulled to failure at $\dot{\varepsilon}=1{\cdot}4\times10^{-3}\ s^{-1}$ and at various temperatures

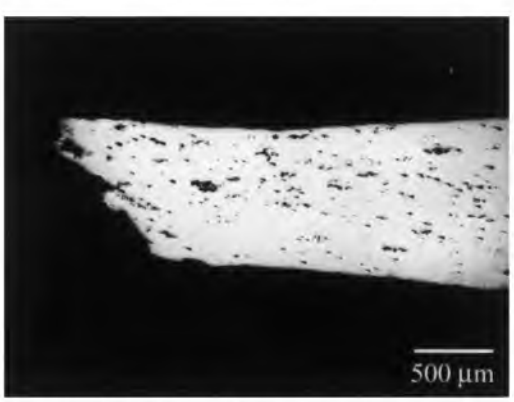

5 Cross-sectional views of the fractured sample strained at $\dot{\varepsilon}=1{\cdot}4\times10^{-3}\ s^{-1}$ and T=475°C

the pseudo-brittle fracture associated with cavitation occurs (Fig. 4). Notably, fracture tips are placed at an angle of about 45° to the tension axis (Fig. 5).

Figure 6 shows plots of flow stresses taken at a true strain of about 0·4, the coefficient of strain rate sensitivity m and elongation to failure δ as functions of initial strain rate. It is seen that at all of the temperatures, the σ–ε curves show evidence of a sigmoidal shape (Fig. 6*a*) with the maximum strain rate sensitivity coefficient m at a strain rate of $1{\cdot}4\times10^{-3}\ s^{-1}$ (Fig. 6*b*). The highest superplastic ductility of 960% is observed at this strain rate at 475°C (Fig. 6*c*) with the

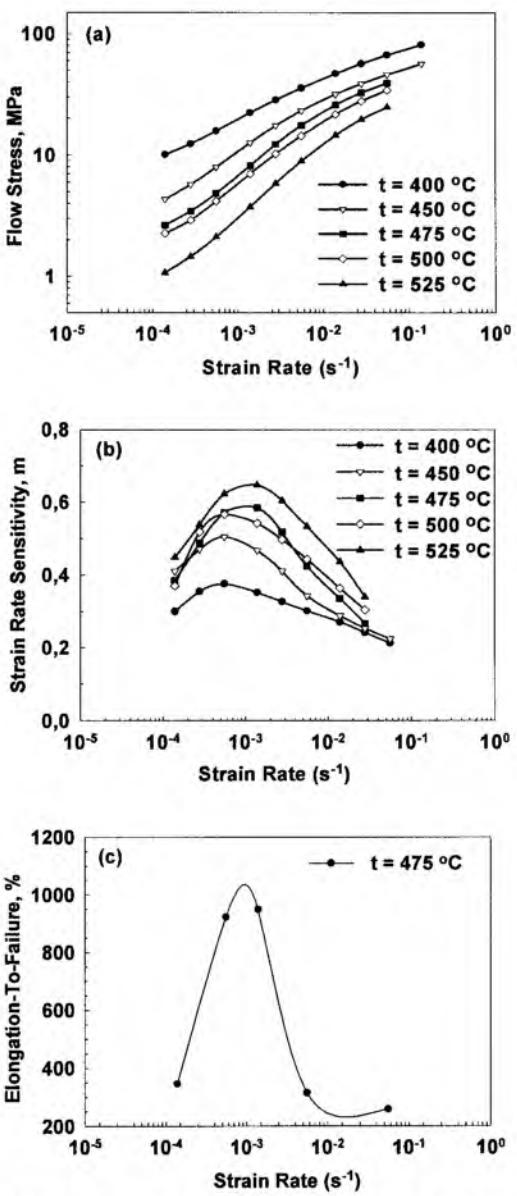

6 Variation of (a) flow stress σ taken at $\varepsilon\approx0{\cdot}4$, (b) coefficient of strain rate sensitivity m taken at $\varepsilon\approx0{\cdot}4$ and (c) elongation-to-failure δ with strain rate

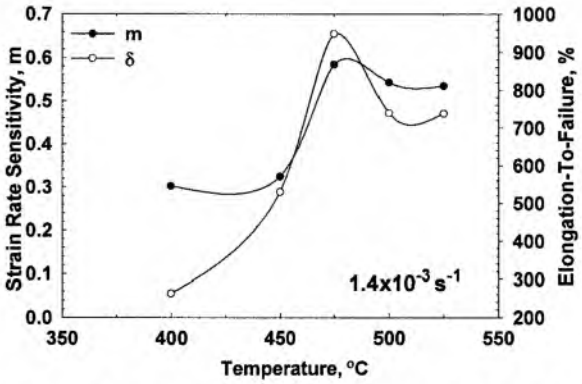

7 Elongation to failure δ and coefficient of strain rate sensitivity m as functions of temperature at $\varepsilon = 1{\cdot}4 \times 10^{-3}\ s^{-1}$

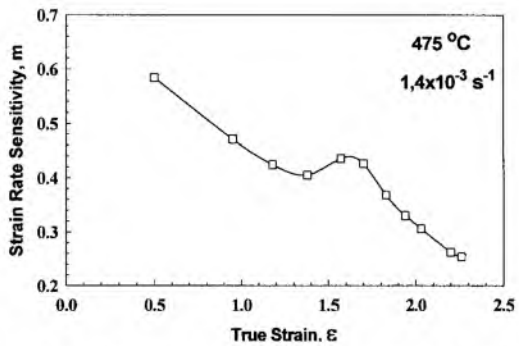

8 Effect of strain on coefficient of strain rate sensitivity m at $\dot{\varepsilon} = 1{\cdot}4 \times 10^{-3}\ s^{-1}$

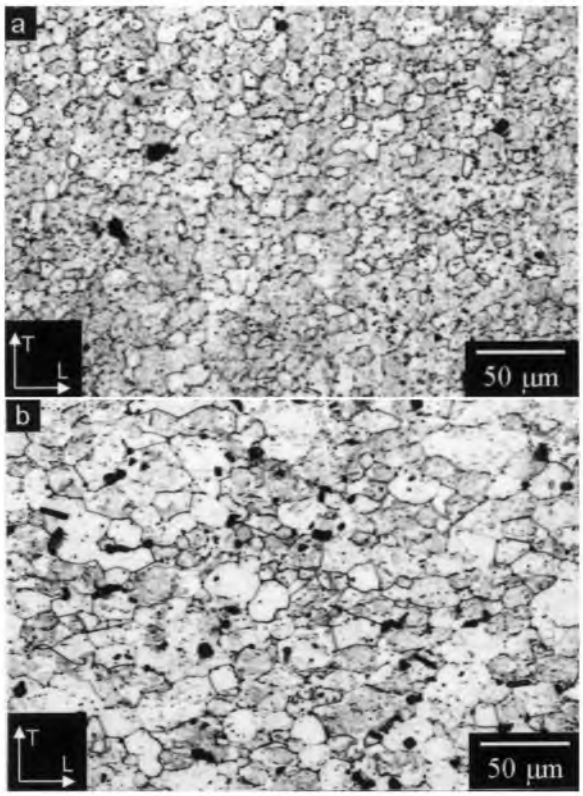

9 Microstructure of the 1443 Al after superplastic deformation at 525°C and $\varepsilon = 1{\cdot}4 \times 10^{-3}\ s^{-1}$ (a) after static annealing for 6300 s (1·75 h) in grip section and (b) after $\varepsilon \approx 2{\cdot}1$ in gauge section

corresponding $m \approx 0{\cdot}58$. At the same time, the highest m value (0·64) was found at a similar strain rate and 525°C, at which $\delta \approx 750\%$. However, the optimum strain rate for superplasticity, at which the highest m values appear, remains essentially unchanged. Increasing temperature results in decreasing flow stress and increasing m value. At a fixed strain rate of $1{\cdot}4 \times 10^{-3}\ s^{-1}$, the m value and ductility grow with increasing temperature at $T \leqslant 475$°C (Fig. 7). Upon further temperature increase the m and δ values slightly decrease.

The coefficient of strain rate sensitivity tends to decrease with increasing strain at optimum superplastic conditions (Fig. 8).

Microstructural evolution

The microstructural evolution of the 1443 Al was studied under both static (grip section) and dynamic (gauge section) annealing in the temperature range 400–525°C. Grain sizes observed after static annealing L_s, dynamic annealing L_d and the grain aspect ratio AR, defined as the ratio of the grain dimension in the tension direction to that in the transverse direction, are summarised in Table 1. At $T \leqslant 500$°C, grained structure after TMP is stable under static annealing (Table 1). Extensive grain growth was found at $T = 525$°C (Table 1, Fig. 9).

Figure 10 shows microstructures at high magnifications. It is pointed out that most of the coarse dark phases located along grain boundaries were (Fig. 10) holes resulting from the fall-out of the S-phase under foil preparation. Particles with an equiaxed shape and sited along grain boundaries were identified as S-phase by the diffraction technique (Fig. 11), and particles with a rodlike shape and located within grain interiors were identified as T_B-phase. Notably in the temperature interval 400–475°C about 25% of grain boundaries were free from precipitations of S-phase. Volume fraction and mean size of $Al_3(Zr,Sc)$ and Al_2CuMg (the S-phase) dispersoids after static annealing are summarised in Table 2. It is seen that after static annealing at 400°C, the volume fraction of the S-phase increases three-fold in comparison with the initial state (Fig. 1) and therefore the S-phase precipitates during static annealing. In

Table 1 Average grain size after static annealing L_s, superplastic deformation L_d and the aspect ratio of grains AR in 1443 alloy strained up to failure at a strain rate of $1{\cdot}4 \times 10^{-3}\ s^{-1}$ in the temperature interval 400–525°C

T, °C	400	450	475	500	525
Local strain in gauge sections (the equivalent time of static annealing in grip sections, h)	ε = 1·3 (0·62)	ε = 1·8 (1·21)	ε = 2·3 (2·14)	ε = 2·1 (1·75)	ε = 2·1 (1·75)
L_s, μm	11·4	11·5	11·8	11·9	19·6
L_d, μm*	15·1/9·2	15·6/9·5	17·4/10·8	23·0/17·3	24·0/19·2
AR	1·64	1·64	1·61	1·33	1·25

*Numerator and denominator are grain sizes measured in the longitudinal (tension) and transverse directions, respectively.

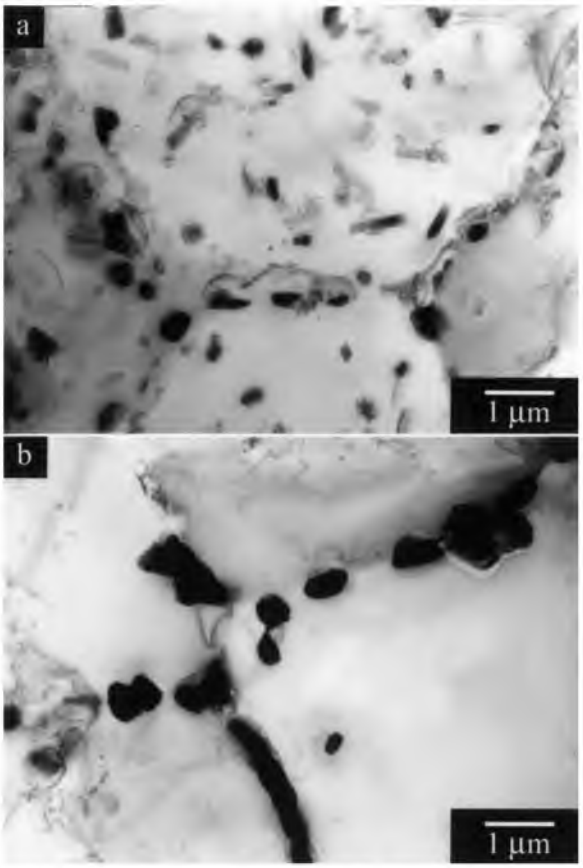

10 Appearance of the microstructure at a high magnification for the samples subjected to static annealing at (a) 400°C for 2232 s (0·62 h) and (b) 475°C for 7704 s (2·14 h)

the temperature interval 400–475°C the increasing temperature leads to complete dissolution of the T_B-phase, and coagulation and partial dissolution of the S-phase takes place (Table 2, Fig. 10). Almost complete dissolution of the S-phase was found at $T=525$°C (Fig. 9*a*, Table 2). The retaining particles of the S-phase are coagulated (Fig. 9*a*) and could not contribute to Zener drag pressure. Therefore, remarkable static grain growth, which starts to occur at $T>475$°C, associates with dissolution of S-phase located along grain boundaries. It is worth noting that the size and volume fraction of $Al_3(Zr,Sc)$ dispersoids remain virtually unchanged (Table 2).

Significant grain elongation along the tension axis was observed at all temperatures of superplastic deformation and remarkable grain growth was found at $T\geqslant475$°C (Table 1, Figs. 9*b* and 12). In the temperature interval 400–475°C the dynamic grain size and AR values are independent on temperature (Table 1). At these temperatures, high grain elongation ($AR\approx1·6$)

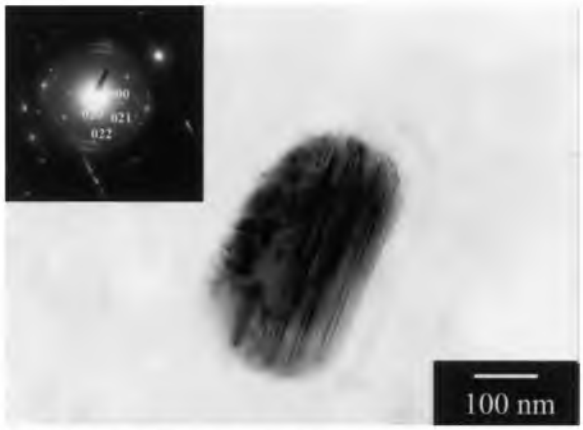

11 Bright field image showing the presence of S-phase (Al_2CuMg)

suggests significant contribution of dislocation glide to total deformation.[5,16,17] At $T>475$°C, the AR value ($\leqslant1·33$) is typical for standard superplastic alloys with high contributions of grain boundary sliding (GBS) to the total elongation.[5,16] It is worth noting that superplastic deformation results in the formation of coarse particles of the S-phase sited on grain boundaries (Fig. 12*c*), and at 525°C, coarse particles of T_B-phase with platelike morphology could be recognised (Fig. 9*b*).

An unusual effect of strain on microstructure was found at the optimal temperature and strain rate of superplastic deformation (Fig. 12). An extensive grain growth associated with steady-state flow ($\varepsilon\approx1·4$) led to the formation of coarse grains with sizes of 21·1 and 13·7 μm in tension and transverse direction, respectively (Fig. 12*b*). It is worth noting that S-phase particles can be found within the interiors of grains (Fig. 12*b*), which is in contrast with initial state (Fig. 12*a*) and after fracture (Fig. 12*c*), where the particles are sited mostly on grain boundaries. Upon further strain a grain refinement as a result of dynamic recrystallisation occurred resulting in grain sizes of 17·4 and 10·8 μm in tension and transverse direction, respectively. It is apparent that strain softening could be attributed to this grain refinement. This assumption is supported by a minor increase in the m value upon strain softening ($\varepsilon=1·5$–$1·8$) (Fig. 8). At $\varepsilon>1·8$, the decreasing m coefficient with strain (Fig. 8) could be associated with concurrent grain elongation and growth leading to the establishment of secondary strain hardening and termination of superplastic deformation. Thus, the fine-grained structure in the 1443 Al is unstable under superplastic deformation at $T\geqslant475$°C. However, at 475°C and probably at 525°C, strain-induced grain growth leading to grain coarsening is superseded by dynamic recrystallisation providing grain refinement. As

Table 2 Zener drag pressure P_z calculated for $Al_3(Sc,Zr)$ dispersoids and S-phase (Al_2CuMg), and their average size D_p and volume fraction V in the 1443 alloy

		Static annealing at		
	Initial state after TMP	400°C	475°C	525°C
D_p, nm*	34/–	34/260	34/520	43/–
V, %*	0·50/–	0·41/1·43	0·42/1·13	0·52/–
P_z, N m^{-2}*	$1·3\times10^5$/–	$1·1\times10^5$/$7·7\times10^5$	$1·1\times10^5$/$1·8\times10^5$	$1·1\times10^5$/–

*The figure to the left of the oblique denotes $Al_3(Sc,Zr)$ dispersoids and that to the right denotes S-phase (Al_2CuMg)

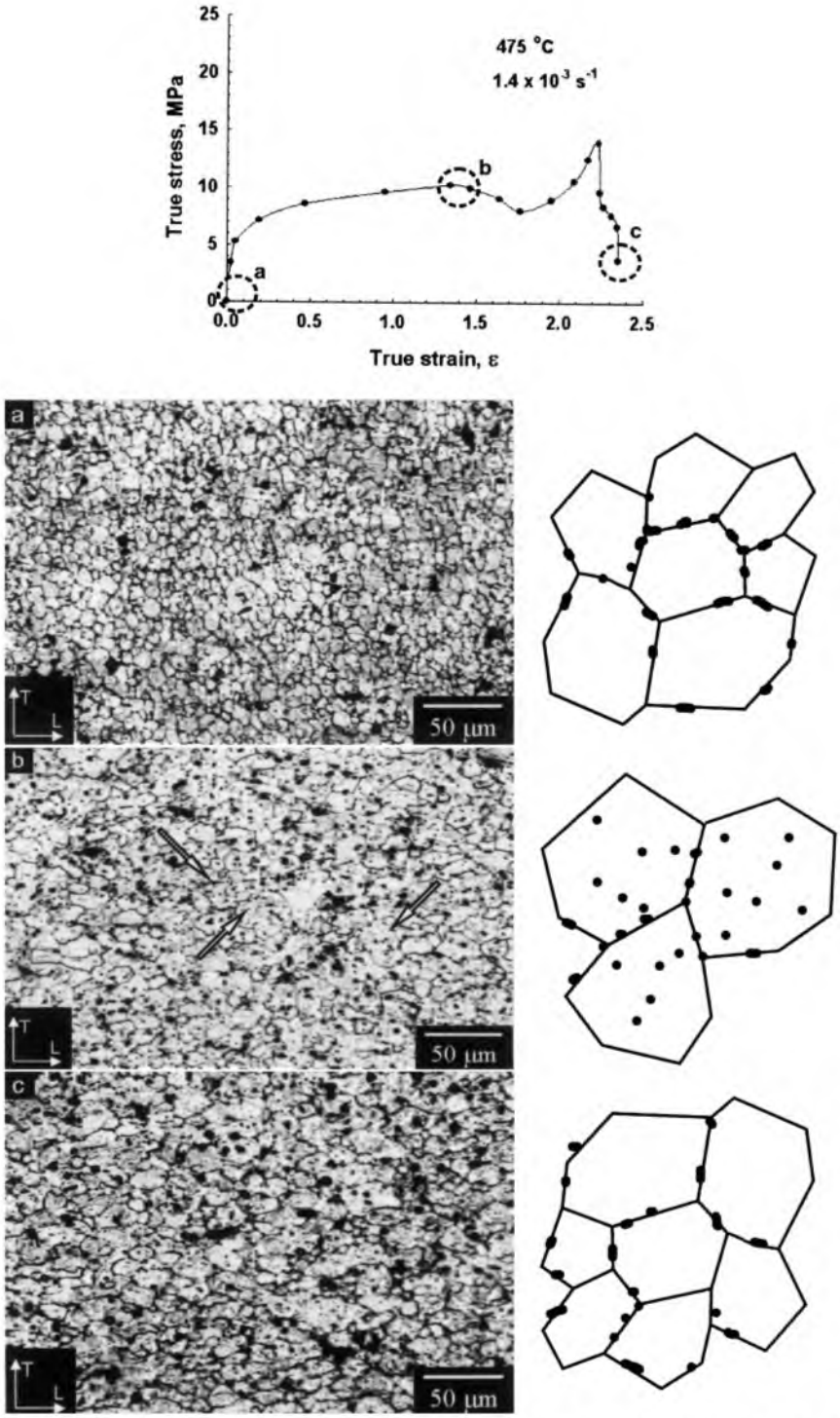

12 Microstructures and their schematic representation evolved at different stages of superplastic deformation at 475°C and $\dot{\varepsilon}=1{\cdot}4\times10^{-3}$ s^{-1}. Arrows indicate particles of the S-phase within grains

a result, the final grain sizes and the grain size after static annealing are essentially the same. At 500°C, dynamic recrystallisation is superseded by secondary grain growth and extensive dynamic grain growth could be found on samples strained up to failure. Unusual microstructure evolution can induce transition from steady-state flow to strain softening followed by secondary strain hardening (Fig. 12).

Cavitation

The average size of cavities A, coefficient of cavity aspect ratio CAR, and porosity volume fraction V in the 1443 Al after superplastic deformation are presented in Table 3. Large cavities with an irregular, jagged shape are observed (Fig. 13), suggesting plasticity controlled cavity growth. Their fraction tends to increase with strain. No fine cavities exhibiting equiaxed shape, which suggests diffusion controlled growth, were found.[5,16] It is pointed out that most of the dark phases in Fig. 13*b* might be the coagulated T_B and S-phases. Notably, even at $T=525$°C, the volume fraction of pores in the samples strained to failure is significantly less than $\approx8\%$, which is a critical value resulting in fracture as a result of cavitation.[5,16] No cavity interlinkage was found also.

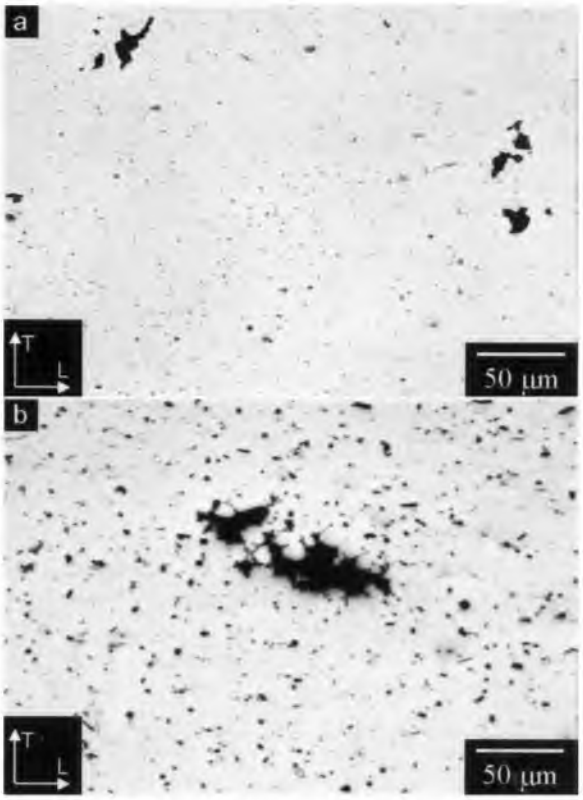

a 475°C at $\varepsilon \approx 2{\cdot}3$; *b* 525°C at $\varepsilon \approx 2$

13 Cross-sectional view of samples strained at $\dot{\varepsilon} = 1{\cdot}4 \times 10^{-3}\ s^{-1}$

The failure in the 1443 Al results from crack propagation between large pores with irregular shape at an angle of ≈45° to the tension axis (Fig. 5). Therefore, an increase in temperature leading to the formation of coarse voids with irregular shape facilitates the process of crack nucleation. This is why at $T \geqslant 500$°C, superplastic ductility tends to decrease with increasing temperature despite the fact that the highest m value appears at these temperatures (Fig. 6*b*).

Discussion

The Zr and Sc additions to the 1443 Al resulted in the formation of $Al_3(Zr,Sc)$ type dispersion particles.[18] The ratio between Sc and Zr as 2·7:1 resulted in incoherent dispersoids, which could not serve as effective pinning agents for climbing dislocations. As a result, in the 1443 Al the recrystallised structure was evolved during rapid recrystallisation annealing followed by warm working. However, a dispersion of these particles exerts a retarding force on migrating high-angle boundaries and this has a profound effect on the stability of the recrystallised structure under static and dynamic annealing.[10] In addition, the precipitations of the S-phase, which are characterised by low solubility during static annealing in the temperature interval 400–475°C, can effectively pin grain boundaries.

Table 3 Average cavity size *A*, coefficient of cavity aspect ratio CAR, and porosity volume fraction *V*, of the 1443 alloy strained up to failure at various temperatures and at $\dot{\varepsilon} = 1{\cdot}4 \times 10^{-3}\ s^{-1}$

T, °C	400	450	475	500	525
A, μm*	3·7/2·6	5·2/3·4	10·1/6·6	11·4/6·6	37·4/18·5
CAR	1·4	1·5	1·5	1·7	2·0
V, %	0·42	0·48	0·87	1·08	2·45

*Numerator and denominator represent cavity sizes measured in the longitudinal and transverse directions, respectively.

To evaluate the effect of the $Al_3(Zr,Sc)$ and Al_2CuMg particles on grain stabilisation under static annealing, the Zener drag pressure was evaluated. It was assumed that all $Al_3(Zr,Sc)$ dispersoids have incoherent origin. It is known that coherent particles are twice as effective in pinning a grain boundary as incoherent particles of the same size.[10] However, taking into account the negligible fraction of coherent $Al_3(Zr,Sc)$ dispersoids (≈7%) and low accuracy of evaluation of the Zener drag force this fact was discarded. Restraining force originated from T_B-phase was also discarded because of low volume fraction of this phase.

The Zener drag pressure P_z was evaluated for $Al_3(Zr,Sc)$ dispersoids assuming a random distribution of particles according to the procedure described in Refs. 10 and 19. The following expression was used[19]

$$P_z = \frac{3}{2} f \frac{\gamma}{R} \tag{1}$$

where f is the volume fraction of particles, γ is the grain boundary energy taken as 0·3 Nm^{-1} (Ref. 20) and R is the radius of particles. Particles from the S-phase precipitate on existing grain boundaries. The Zener drag pressure for Al_2CuMg dispersoids was evaluated in accordance with the schema presented in Fig. 3.22*d* from Ref. 10 using equation

$$P_z = \frac{D\gamma f}{4R^2} \tag{2}$$

where D is the grain size. Equations (1) and (2) were used with the presumption that $Al_3(Zr,Sc)$ and Al_2CuMg particles exhibit equiaxed shape.

Calculations of the drag pressure are summarised in Table 2. It is seen that the Zener pressure originating from Al_2CuMg dispersoids gives a significant contribution to the total drag force in the temperature interval 400–475°C. The precipitations of the S-phase increase the Zener drag pressure by a factor of about 2, providing high stability of fine grains under static annealing. It is seen that the Zener drag force is sufficient to stabilise grain structure with an average grain size of ≈11 μm under static annealing at $T \leqslant 475$°C. Dissolution of S-phase with increasing temperature leads to a remarkable decrease in the restraining force (Table 2). As a result, at $T \geqslant 500$°C, extensive static grain growth starts to occur.

In the temperature interval 400–500°C, strain-induced migration of high-angle boundaries takes place because of the non-random distribution of Al_2CuMg particles (Fig. 12*a*). High-angle boundaries, which were free from chains of the S-phase, can migrate. In addition, some high-angle boundaries, along which the low number of S-phase particles precipitated, can detach from chains of these dispersoids. Upon further migration only the $Al_3(Zr,Sc)$ dispersoids exert the Zener pinning pressure. This pinning force is not enough to retard grain growth. A boundary migrates up to a point where a chain of the S-phase particles is sited, i.e. up to the opposite grain boundary (Fig. 12*b*), and next, the migration ceases. This is why the grain size increases by a factor of two at initial stages of superplastic deformation and chains of the S-phase were

observed within grains (Fig. 12*a* and *b*). The work hardening associates with this dynamic grain growth (Fig. 12).[5] Steady-state flow takes place if the increased grain size remains essentially stable (≈20 μm at 475°C and $\dot{\varepsilon}=1{\cdot}4\times10^{-3}\ s^{-1}$). Accumulation of lattice dislocations within these relatively coarse grains leads to dynamic recrystallisation providing grain refinement (Fig. 12*c*) and strain softening. This process can repeat.

Heterogeneous precipitations of the S-phase along grain boundaries during static annealing therefore result in unusual σ–ε curves in the Al–Li–Cu–Mg alloy at the optimal superplastic conditions.

Conclusions

An Al–1·9%Li–1·7%Cu–1%Mg alloy containing nanoscale $Al_3(Sc,Zr)$ dispersoids can be thermomechanically processed into a uniform fine grained (≈11 μm) structure. The 1443 alloy exhibits superplasticity in the temperature interval 400–525°C with the highest elongation to failure (960%) at 475°C and $\dot{\varepsilon}=1{\cdot}4\times10^{-3}\ s^{-1}$. During superplastic deformation the grain growth is superseded by grain refinement, which leads to alternation of strain hardening, steady-state flow and strain softening stages.

References

1. I. N. Fridlyander: *Met. Sci. Heat Treat.*, 2001, **1**, 5–9.
2. I. N. Fridlyander, K. V. Chuistova, A. L. Berezina and N. I. Kolobnev: 'Aluminum–lithium alloys. structure and properties', 155–176; 1992, Kiev, Naukova Dumka.
3. M. Shagiev, Y. Motohashi, F. Musin, R. Kaibyshev and G. Itoh: *Mater. Trans.*, 2003, **44**, 1694–1697.
4. M. Shagiev, Y. Motohashi, F. Musin, R. Kaibyshev and G. Itoh: *Mater. Trans.*, 2003, **44**, 1698–1701.
5. J. Pilling and N. Ridley: 'Superplasticity in crystalline solids'; 1989, London, The Institute of Metals.
6. Q. Liu, X. Huang, M. Yao and J. Yang: *Acta Metall. Mater.*, 1992, **40**, 1753–1762.
7. H. P. Pu, F. C. Liu and J. C. Huang: *Metall. Mater. Trans.*, 1995, **26A**, 1153–1166.
8. J. C. Huang and T. H. Chuang: *Mater. Chem. Phys.*, 1999, **57**, 195–206.
9. H. P. Pu and J. C. Huang: *Scr. Met. Mater.*, 1995, **33**, 383–389.
10. F. J. Humphreys and M. Hatherly: 'Recrystallisation and related annealing phenomena'; 1996, Oxford, Pergamon Press.
11. R. Kaibyshev, A. Goloborodko, F. Musin, I. Nikulin and T.Sakai: *Mater. Trans.*, 2002, **43**, 2408–2414.
12. R. Grimes, W. S. Miller and R. G. Butler: *J. Phys. Colloq.*, 1987, **48**(C3), 239–249.
13. T. G. Nieh, L. M. Hsiung, J. Wadsworth and R. Kaibyshev: *Acta Mater.*, 1998, **46**, 2789–2800.
14. R. Kaibyshev, K. Shipilova, F. Musin and Y. Motohashi: *Mater. Sci. Technol.*, 2005, **21**, 408–418.
15. R. Kaibyshev, F. Musin, D. Gromov, T. G. Nieh and D. R. Lesuer: *Mater. Sci. Technol.*, 2003, **19**, 483–490.
16. O. A. Kaibyshev: 'Superplasticity of alloys, intermetallides, and ceramics'; 1992, Berlin, Springer-Verlag.
17. R. Kaibyshev, F. Musin, D. R. Lesuer and T. G. Nieh: *Mater. Sci. Eng.*, 2003, **342**, 169–177.
18. V. G. Davydov, V. I. Elagin, V. V. Filatova and T. D. Rostova: *Mater. Sci. Heat Treat. Met.*, 1996, **8**, 25–30.
19. E. Nes, N. Ryum and O. Hunder: *Acta Metall.*, 1985, **33**, 11–22.
20. F. Murr: 'Interfacial phenomena in metals and alloys'; 1975, Reading, MA, Addison-Wesley.